BIBECHANA
Vol. 22, No. 2, August 2025, 108-115

ISSN 2091-0762 (Print), 2382-5340 (Online)
Journal homepage: http://nepjol.info/index.php/BIBECHANA
Publisher:Dept. of Phys., Mahendra Morang A. M. Campus (Tribhuvan University)Biratnagar

Structural characterization of HDAC2-MTA1 complex

Narayan Gautam[1,2], Narayan P. Adhikari[1]

[1] *Central Department of Physics, Tribhuvan University, Kirtipur, Nepal*
[2] *Tri-Chandra Multiple Campus, Tribhuvan University, Kathmandu 44613, Nepal*
*Corresponding author. Email:narayan.adhikari@cdp.tu.edu.np

Abstract

Histone deacetylases are recruited to specific transcriptional repression complexes through interactions with corepressor proteins. This recruitment leads to chromatin condensation and transcriptional silencing. In this study, we modeled the complex structure of HDAC2 with MTA1 and investigated the HDAC2 and MTA1 interactions using all-atom molecular dynamics (MD) simulation. Our results show that the ELM2-SANT domains of MTA1 wrap completely around HDAC2. We identified the different types of interactions such as hydrogen bonds, salt bridges, and hydrophobic interactions. Specifically, GLU186, GLU147, GLU163, LYS166, and LYS124 amino acid residues of HDAC2 form both hydrogen bond and salt bridge interactions with ARG168, ARG189, ASP187, and GLU195 amino acid residues of MTA1. Additionally, TYR15 amino acid of HDAC2 form hydrogen bonds with GLU195 amino acid of MTA1. In addition to hydrogen bond and salt bridge interactions, we also analyzed hydrophobic interaction.

Keywords

HDAC2, MTA1, Molecular dynamics simulation, Salt bridge, Hydrogen bonding, Hydrophobic interactions, Solvent-accessible surface area, MM-GBSA

Article information

Manuscript received: January 19, 2025; Revised: February 6, 2025; Accepted: February 10, 2025
DOI https://doi.org/10.3126/bibechana.v22i2.74254

1 Introduction

Nucleosomes are the basic units of chromatin that consist of histone and non-histone proteins in eukaryotic cells. DNA is wrapped around histones that help the DNA fit into the nucleus. Transcription factors are proteins that interact with the DNA and help to remodel the chromatin structure by repressing or expressing the transcription. When the lysine residues on the amino-terminal of histone are acetylated, the interaction between the histones and DNA is weakened, and the chromatin is accessible for the transcription. The acetylation is possible due to the enzyme HATs. When the acetyl group is removed with the help of HDACs from the lysine of histones on the amino-terminal, the interaction of the histone with DNA is strengthened. At that time, the chromatin is inaccessible for the transcription.

Many studies have predicted that there is an important link between HDACs and cancer. HDAC-related interactions are known to be associated with transcriptional repression of some genes, and abnormal recruitment of HDACs to their promoter is con-

tributed to the tumorgenesis. HDAC (NuRD complex) with that of MTA1 have indicated a possible function of HDACs in tumor progression. MTA1 also physically interacts with HDAC1. MTA1 is a target of heregulin (HRG) and plays a significant role in the repression of estrogen receptor (ER)-mediated transcription by recruiting HDACs [1]. The metastatic is regulated by different genes. Out of these genes, MTA proteins play crucial roles in the development and spread of cancer cells [2, 3].

Histone modification is one of the important epigenetic modifications that is essential for the regulation of gene expression. Histone deacetylases (HDACs) are enzymatic proteins that remove acetyl groups from histone and non-histone proteins which repress the gene expression [4, 5]. HDACs are associated with different biological processes such as cellular proliferation, apoptosis, and signal transduction [6, 7]. Overexpression and abnormal expression of HDACs to their promoter causes different types of diseases such as cancer, neurodegenerative disorders, HIV, diabetes, inflammation and cardiac diseases [8]. The inhibition of histone deacetylases (HDACs) results in increased acetylation of histones and various non-histone proteins, encompassing signaling mediators [9, 10], tumor suppressors [11], transcription factors [12], and DNA repair proteins [13]. There are 18 members in the HDAC family, divided into 4 classes based on their structure and function [14]. Class I includes HDAC1-3 and 8; class II includes HDAC4-7, 9, and 10; class III includes sirtuin enzymes (SIRT 1-7); and class IV comprises only HDAC11, which is structurally different from the others. Within class II, there are further subdivisions: class IIa (HDAC4, 5, 7, and 9) and class IIb (HDAC6 and 10), based on their subcellular localization and expression patterns. Histone deacetylases 1 and 2 are required for brain development [15] and heart development [16].

The different types of MTA proteins are MTA1, MTA2, and MTA3 [17, 18]. MTA1 and MTA2 are expressed ubiquitously but the expression pattern of MTA3 is restricted. MTA1 and MTA2 are mainly found in the nucleus [19]. MTA1 was originally identified through from rat metastatic breast tumors [20] after that it was found that MTA1 is widely up-regulated in human tumors [21]. MTA1, MTA2, including HDAC1, HDAC2 are the subunits of NuRD complex that provide the essential role of MTA and HDACs proteins to the chromatin modification [22, 23]. There are different domains in the MTA1 protein. Bromo-adjacent-homology (BAH) domain, the EGL-27 and MTA1 homology 2 (ELM2) domain, and the SWI3, ADA2, N-CoR, and TFIII-B (SANT) domains are the important domains [18]. After recruiting HDACs, the ELM2 domain functions as a transcriptional repression domain [24]. The ELM2 and SANT domain of the MTA1 establish numerous interactions with the HDAC [1, 25]. The structure of HDAC1 in complex with MTA1 from the NuRD complex was reported by Millard and coauthors in 2013. They reported that ELM2-SANT domains from MTA1 wrap completely around HDAC1 [25]. HDAC2 contains many domains with defined functions. The catalytic domain common to all class I HDACs is formed by a stretch of more than 300 amino acids constituting a large portion of the protein [26]. A nuclear localization signal (NLS) at the C-terminus can only be found in HDAC1 [27], whereas a C-terminal coiled-coil domain (possibly enabling additional protein-protein associations) seems to be specific for HDAC2 [6]. Despite previous research into interactions between HDAC2 and MTA1 [25], the precise nature of the HDAC2-MTA1 functional complex remains unknown. We used all-atom molecular dynamics (MD) simulations to investigate the interactions of HDAC2 and MTA1. MD simulations and in silico studies have successfully been used to investigate the molecular interactions, including HDACs [28, 29]. First, we predicted the structure of the HDAC2-MTA1 complex and performed MD simulations to investigate the HDAC2-MTA1 interactions. We identified the binding sites and crucial residues and estimated the key parameters related to the structural stability and binding affinity of the complex.

2 Methods

2.1 System preparation

The structure of the HDAC2-MTA1 complex was predicted with AlphaFold2 Colab [30] using the FASTA sequences of HDAC2 (UniProt [31] accession ID Q92769) and MTA1 (UniProt [31] accession ID Q13330). HDAC2 and MTA1 proteins have 488 and 715 amino acids, respectively. The AlphaFold2 prediction of the HDAC2-MTA1 complex was obtained with full-length sequences for HDAC2 and MTA1.

2.2 MD simulations

We utilized the NAMD software [32] and the CHARMM36m force field [33] to conduct all-atom MD simulations of the HDAC2-MTA1 complexes, as employed in previous studies [28, 29, 34]. The simulation input files were prepared using the CHARMM-GUI web server [35]. In cubic boxes, the systems were solvated with a TIP3 water model and 150 mM NaCl. The HDAC2-MTA1 complex, after being solvated and ion-neutralized, contained a total of 139681 atoms. The system was minimized for 10,000 steps with heavy atoms being harmonically restrained, followed by an equilibration of 100

picoseconds using the NVT ensemble. The production runs were performed using a time step of 2 femtoseconds.

2.3 Data analysis

The VMD software [36] was utilized to analyze simulation trajectories. ChimeraX [37] and VMD were utilized to effectively visualize protein structures and generate high-quality figures. The binding free energy was calculated using the MM/GBSA approach with NAMD, as described in previous publications [28, 29, 34]. The equation used to estimate binding free energy for the complex is as followed with the entropy term ignored [38]:

$$\Delta G = G_{HDAC2-MTA1} - G_{HDAC2} - G_{MTA1} \quad (1)$$

where, $G_{HDAC2-MTA1}$ or G_{HDAC2} or G_{MTA1} is the sum of energy contributions due to internal (bond, angle, dihedral, and improper), electrostatic, van der Waals, and solvation (polar and non-polar contributions) energies ($G = E_{internal} + E_{electrostatic} + E_{vdw} + E_{solvation}$). A contact distance cutoff of 3.5 Å and an angle cutoff of 30 degrees were used to analyze hydrogen bonding, and the same atomic distance cutoff was used to analyze salt bridges. Contact surface area was calculated using the formula [39]:

$$ContactArea = \frac{SASA_{HDAC2} + SASA_{MTA1} - SASA_{HDAC2-MTA1}}{2} \quad (2)$$

where, $SASA_{HDAC2}$ corresponds to solvent-accessible surface area (SASA) of HDAC2 at any time, $SASA_{MTA1}$ to SASA of MTA1, and $SASA_{HDAC2-MTA1}$ to SASA of the complex. VMD was used to measure the SASA values using the simulation trajectories.

3 Results and Discussion

We used AlphaFold2 to predict the molecular structure of the HDAC2-MTA1 complex and performed MD simulations to study into how the complex formed between HDAC2 and the MTA1 protein. To evaluate the structural stability of the predicted complex and identify the crucial residues that contribute to the formation, we performed an MD simulation. Additionally, we calculated the binding free energy and contact surface area of the HDAC2-MTA1 complex.

3.1 Prediction of the HDAC2-MTA1 complex

Figures 1(a) and 1(b) illustrate the individual complete structures of HDAC2 and MTA1 proteins predicted from AlphaFold2 respectively. Although the MTA1 protein exhibits a highly disordered structure with unstructured loops, HDAC2 has a more stable structure. Figure 1(c) illustrates the HDAC2-MTA1 complex structures predicted by AlphaFold2. This predicted model's interface predicted template modeling (ipTM) score is 0.76. Model confidence is typically associated with an ipTM score of 0.75 or higher [40]. To the best of our knowledge, the specific HDAC2 amino acids that interact with MTA1 have not yet reported. We were able to predict the structure of the HDAC2-MTA1 complex by giving Alphafold2 a full-length sequence of both HDAC2 and MTA1. The HDAC2-MTA1 complex included a full-length HDAC2 and MTA1 sequence, as illustrated in Figure 1(c). A robust cutoff of 5 Å is effective in establishing solid foundations of the Protein Structure Networks approach [41]. The amino acids in the MTA1 protein strongly interact with HDAC2 in several areas, including the helix, the beta sheet, and the unstructured loops. To make the system as small as possible, we removed unstructured loops and helices that were away from more than 5 Angstroms from where the HDAC2 and MTA1 meets as shown in figure 1(d). This truncation significantly reduces the size of the system as well as the computational cost. Subsequently, we performed a 500 ns MD simulation of the complex that included all atoms.

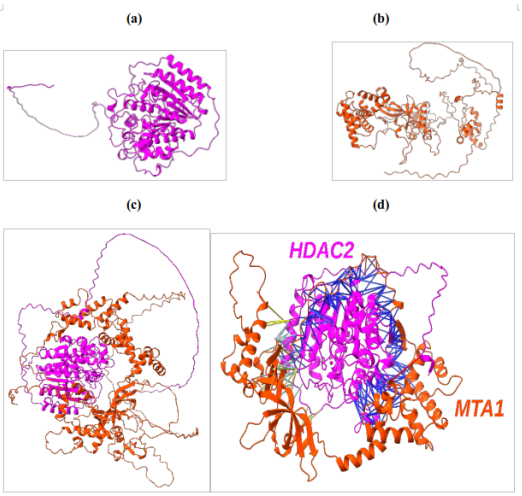

Figure 1: (a) Structure of HDAC2 (b) Structure of MTA1(c) Modeled Structure of HDAC2-MTA1 Complex; (d) Structure of the HDAC2-MTA1 complex after removing the loops beyond five angstroms form each other.

3.2 Structural stability of the HDAC2-MTA1 complex

We monitored the structural stability of the HDAC2-MTA1 complex using RMSD measurements as shown in figure 2(a) and used simulation results to confirm HDAC2-MTA1 complex formation. RMSD plot shows the initial reorganizations until 280 ns, but after that the structural stability of the complex was maintained with relatively stable RMSD measurements. Figure 2(b) shows the structure of the complex after 500 ns of simulation of the HDAC2-MTA1.

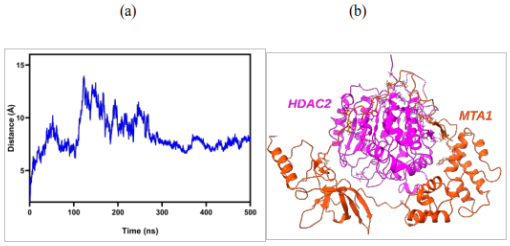

Figure 2: (a) RMSD of the HDAC2-MTA1 complex from the 500 ns simulation trajectory. (b) HDAC2-MTA1 complex structure after 500 ns of simulation time.

3.3 Major interaction involved in the complex formation and stabilization

To understand the mechanism of the interaction of HDAC2 with MTA1, we explored their dynamics during the simulation of the complex. To identify the inter-protein interactions, we evaluated AlphaFold protein-protein interaction with ChimeraX in the predicted complex structure of the HDAC2 and MTA1 that lie within a 5 Angstrom distance in the HDAC2-MTA1 complex. Figure 1(d) shows the structure of the HDAC2-MTA1 complex, in which both proteins are within 5 Angstrom to each other. Alphafold believes that blue color lines have high confidence, which means residue pairs that are close to each other, and red color lines indicate that the residue pairs have low confidence.

3.3.1 Hydrogen bonding between HDAC2 and MTA1

To predict the hydrogen bonds formed between HDAC2 and MTA1, we analyzed the data from the simulation trajectories. This was carried out using the analysis protocol outlined in the methods section. Frequently, a specific amino acid in one protein would form hydrogen bonds with another protein via different atoms. In our simulation, we only took into account individual bonds that were occupying more than 25%. Table 1 displays the occupancies of hydrogen bonds. For each pair of residues, the occupancies presented in Table 1 represent the sum of hydrogen bonding contributions from various atoms within the same residue. The time evolution of each hydrogen bond established by each atom pair from the analysis of the trajectory are shown in Figure 3(a). The types of atoms are shown inside parentheses.

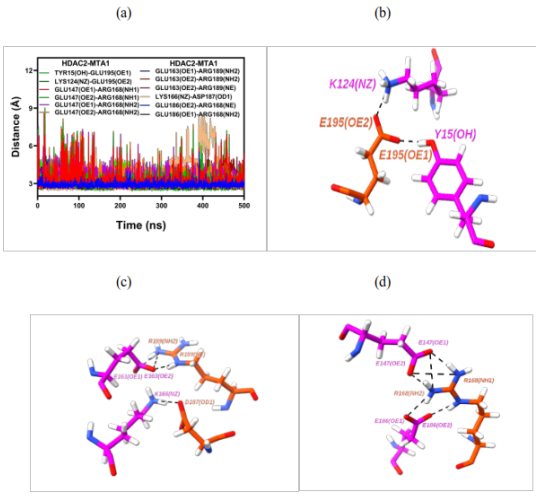

Figure 3: (a) Distance of hydrogen bonds formed between the residues in HDAC2 and MTA1. The type of atoms that are predicted to establish the contacts are provided inside parentheses of each residue. (b) Orientation of residues in both HDAC2 and MTA1 that form the hydrogen bonds. The crucial residues are shown in licorice representation and the black dotted lines represent the hydrogen bonds.

Table 1: Hydrogen bond occupancies obtained from the analysis of trajectories of HDAC2-MTA1 simulation. Except TYR15-GLU195 residues pair, all other residues pairs are involved in the formation of salt bridges as well as hydrogen bonds in the formation of HDAC2-MTA1 protein complex.

HDAC2	MTA1	Occupancy
GLU186	ARG168	156.84%
GLU147	ARG168	137.00%
GLU163	ARG189	130.28%
TYR15	GLU195	63.64%
LYS166	ASP187	58.24%
LYS124	GLU195	46.00%

Table 2: Hydrogen bond length between the atoms of the residues of HDAC2 and MTA1 of the final frame obtained from the 500 ns of the simulation of HDAC2-MTA1 complex

HDAC2 residues	MTA1 residues	Bond-length (Å) (Mean±S.D.)
GLU186(OE2)	ARG168(NE)	2.9±0.17
GLU186(OE1)	ARG168(NH2)	2.9±0.19
GLU147(OE2)	ARG168(NH2)	3.6±0.90
GLU147(OE2)	ARG168(NH1)	3.4±0.79
GLU147(OE1)	ARG168(NH1)	3.3±0.73
GLU147(OE1)	ARG168(NH2)	3.5±0.87
GLU163(OE2)	ARG189(NE)	3.4±0.49
GLU163(OE1)	ARG189(NH2)	3.1±0.38
GLU163(OE2)	ARG189(NH2)	3.2±0.48
TYR15(OH)	GLU195(OE1)	3.2±0.80
LYS166(NZ)	ASP187(OD1)	3.4±1.31
LYS124(NZ)	GLU195(OE2)	2.8±0.26

3.3.2 Contribution of a salt bridge for the formation of the HDAC7-MEF2A complex

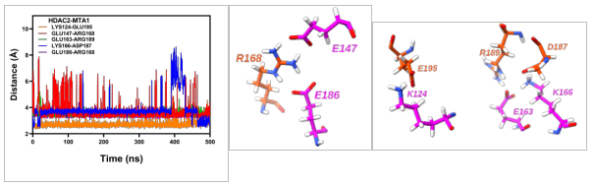

Figure 4: (a) Time evolution of formation of salt bridges between HDAC2 and MTA1 during the complex formation. (b),(c) and (d) Orientation of the residues that formed salt bridges in licorice form.

LYS124 of HDAC2 and GLU195 of MTA1 form a strong salt bridge, despite the hydrogen bond occupancy being relatively low at only 46.00%. This salt bridge is crucial for establishing the linkage between HDAC2 and MTA1, as shown in the figure 4(a) and 4(b) respectively. Three additional salt bridges that we predicted are: GLU147(HDAC2)-ARG168(MTA1), GLU163(HDAC2)-ARG189(MTA1), and GLU186(HDAC2)−ARG168(MTA1), performed nearly equal contributions to the formation of the HDAC2-MTA1 complex. The salt bridges exhibit stability throughout the 500 ns simulation. The remaining salt bridge that we predicted is LYS166(HDAC2)-ASP187(MTA1) and the stability of this salt bridge remains constant throughout the simulation, except for the time period between 380 ns and 410 ns. Figure 4(b) shows the precise orientation of all these residues that form the HDAC2-MTA1 complex within each protein.

3.3.3 Contribution due to hydrophobic interactions

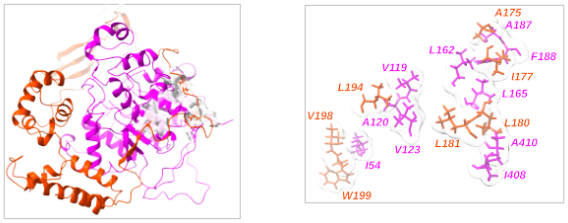

Figure 5: (a) Regions of hydrophobic residues that form hydrophobic interaction between HDAC2 and MTA1, and (b) Hydrophobic residues in HDAC2 (magenta texts) that establish hydrophobic interactions with MTA1 residues (orange red texts) with surface and licorice representation.

The hydrophobic interactions play a crucial role in the formation and stabilization of the complex between HDAC2 and MTA1. Our results show that there are a number of hydrophobic interactions between residues in HDAC2 and MTA1 across the interface. We predicted that hydrophobic residues ILE54, VAL119, ALA120, VAL123, LEU162, LEU165, ALA187, PHE188, ILE408, ALA410 of HDAC2 make hydrophobic interactions with ALA175, ILE177, LEU180, LEU181, LEU194, VAL198, TRP199 of MTA1. Although there are many hydrophobic interactions in the formation of HDAC2-MTA1 complex, the crucial residues that form hydrophobic interaction is shown in figure 5(a). The zoom viewed of figure 5(a) is shown in figure 5(b) in Surface and Licorice representation with Label.

Table 3: The hydrophobic interactions between the different amino acid residues of HDAC2 and MTA1.

HDAC2	MTA1
ILE54	VAL198, TRP199
VAL119	LEU194
ALA120	LEU194
VAL123	LEU194
LEU162	ALA175, ILE177
LEU165	ILE177, LEU180
ALA187	ALA175
PHE188	ILE177
ILE408	LEU180
ALA410	LEU180, LEU181

As shown in figure 5(b), the hydrophobic residues ILE54 of HDAC2 binds strongly with VAL198, TRP199 of MTA1. Three amino acid residues VAL119, ALA120 & VAL123 of HDAC2 make hydrophobic cavity. In that cavity, LEU194 of MTA1 deeply inserted and make strong interaction. Also, IILE177 and ALA175 of MTA1 make hydrophobic interactions with LEU162, ALA187, and PHE188 of HDAC2. Similarly, LEU165, ILE408, and ALA410 of HDAC2 interact with LEU180 and LEU181 of MTA1. We have calculated the hydrophobic contact area of the HDAC2-MTA1 complex by using the equation as described in the method section. Figure 6(a) shows the contact area measurements for the HDAC2-MTA1 complex. We calculated the average and standard deviation (S.D.) of all contact area values (values for each frame of entire 500 ns simulations) as shown in figure 6(a) and obtained 243.89±23.44 Å^2 (Mean±S.D.).

The time evolution of hydrophobic contact area was monitored over a 500 ns molecular dynamics simulation, as shown in figure. At the initial phase, the contact area is stable and is predominantly fluctuated between 200 and 250 Å^2, which represent the relatively stable interactions with minor fluctuations. After 350-500 ns, the contact area is increased, with peak values reaching approximately about 340 Å^2. The higher contact area after 350 ns is due to the formation of new hydrophobic contacts between ILE408 and ALA410 of HDAC2 with LEU180 and LEU181 of MTA1 in the rearrangement of the HDAC2-MTA1 complex. Prior theoretical and experimental research has indicated that burying 1 Å^2 of the hydrophobic surface at the protein-protein interface increases the complex stabilization free energy by -15 ± 1.2 cal/mol. Thus, in the case of the HDAC2-MTA1 complex, the hydrophobic surface area at the HDAC2-MTA1 interface, which measures 243.89 Å^2, plays a significant role in contributing approximately -3.66 kcal/mol to its stability. This suggests that hydrophobic interactions are essential in the formation and stabilization of the HDAC2–MTA1 complex.

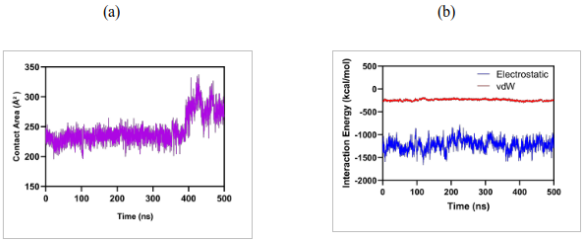

Figure 6: (a) Contact surface area measurements HDAC2 and MTA1 in HDAC2-MTA1 complex, and (b) Time evolution of the non-bonded interaction energy in the HDAC2-MTA1 complex.

We also analyzed two interactions, electrostatic and van der Waals, that help to stabilize HDAC2-MTA1 complex. Electrostatic interactions are due to the charged residues in the proteins. Our result estimated that these interactions are stable after 280 ns of simulation and its value was -1220.25 ± 126.65 kcal/mol. Van der Waals interactions are relatively weaker interactions. These interactions remained stable from the beginning to the end of our simulation. The average strength of the van der Waals interactions was -237.55 ± 20.53 kcal/mol. These negative values of both electrostatic and Van der Waals interaction energy is favorable for the interaction of HDAC2-MTA1. Both non-bonded interaction energies contribute to the stable binding of the HDAC2–MTA1 complex. This observation suggests that HDAC2 and MTA1 form a stable complex through multiple non-covalent interactions.

3.3.4 Binding free energy of the complex

In order to determine the strength of the interaction between HDAC2 and MTA1, we employed the molecular mechanics with a generalized Born and surface area solvation (MM/GBSA) method to calculate the binding free energy of the complex. We have determined the binding free energy of the HDAC2–MTA1 complex using the molecular dynamics (MD) simulation trajectory. The MM/GBSA binding free energy of the HDAC2–MTA1 complex is -223.14 ± 17.71 kcal/mol, indicating a substantial binding free energy for a stable protein–protein complex.

4 Conclusions

The HDAC (NuRD) complex with that of MTA1 have indicated a possible function of HDACs in tumor progression. MTA1 is a target of heregulin (HRG) and plays a significant role in the repression of estrogen receptor (ER)-mediated transcrip-

tion by recruiting HDACs. In this work, we investigated the molecular mechanism of complex formation of HDAC2 with MTA1 protein, using structure predicting tool AlphaFold2 and performed MD simulations. We obtained the HDAC2-MTA1 complex from molecular modeling and assessed its stability using MD simulations. Our results show that HDAC2 interacts with MTA1 through ELM2-SANT domains as in HDAC1-MTA1 interaction. Several hydrogen bonding interactions between the residues at the binding interface are also involved in the binding of HDAC2 and MTA1. In addition to hydrogen bonding, salt bridges between the interfacial charged residues are the also the major interactions involved in the binding. Furthermore, hydrophobic interactions play a significant role in forming and stabilizing the HDAC2-MTA1 complex. Our results reveal that HDAC2 strongly wrapped by MTA1, forming a stable complex via different interactions. Our first structural characterization of the HDAC2–MTA1 complex outlines the molecular basis of the interaction of HDAC2 with MTA1, which offers valuable insights into the recruitment mechanism of the HDAC complex for the transcription repression mediated by MTA1.

Disclosure statement

There are no conflicts to declare.

Author contributions

NPA supervised the project. NG performed the MD simulations and analyzed the data. NG and NPA contributed to the data analysis and interpretation. NG wrote the manuscript NPA contributed to manuscript editing.

References

[1] A. Mazumdar et al. Transcriptional repression of oestrogen receptor by metastasis-associated protein 1 corepressor. 3(1):30–37, 2001.

[2] D. Hanahan and R.A. Weinberg. The hallmarks of cancer. 100(1):57–70, 2000.

[3] N. Sen et al. Role of mta1 in cancer progression and metastasis. 33:879–889, 2014.

[4] P.A. Marks et al. Histone deacetylases and cancer: causes and therapies. 1(3):194–202, 2001.

[5] B. Weinhold. *Epigenetics: the science of change*. National Institute of Environmental Health Sciences, 2006.

[6] I. Gregoretti, Y.-M. Lee, and H.V. Goodson. Molecular evolution of the histone deacetylase family: functional implications of phylogenetic analysis. 338(1):17–31, 2004.

[7] G. Brosch, P. Loidl, and S. Graessle. Histone modifications and chromatin dynamics: a focus on filamentous fungi. 32(3):409–439, 2008.

[8] P. Gediya et al. Histone deacetylase 2: A potential therapeutic target for cancer and neurodegenerative disorders. 216:113332, 2021.

[9] Z.-l. Yuan et al. Stat3 dimerization regulated by reversible acetylation of a single lysine residue. 307(5707):269–273, 2005.

[10] H. Kook et al. Cardiac hypertrophy and histone deacetylase–dependent transcriptional repression mediated by the atypical homeodomain protein hop. 112(6):863–871, 2003.

[11] A. Ito et al. Mdm2–hdac1-mediated deacetylation of p53 is required for its degradation. 2002.

[12] J. Luo et al. Acetylation of p53 augments its site-specific dna binding both in vitro and in vivo. 101(8):2259–2264, 2004.

[13] G. Marzio et al. E2f family members are differentially regulated by reversible acetylation. 275(15):10887–10892, 2000.

[14] N. Sengupta and E. Seto. Regulation of histone deacetylase activities. 93(1):57–67, 2004.

[15] J. Jaworska, M. Ziemka-Nalecz, and T. Zalewska. Histone deacetylases 1 and 2 are required for brain development. 59(4-6):171–177, 2015.

[16] R.L. Montgomery et al. Histone deacetylases 1 and 2 redundantly regulate cardiac morphogenesis, growth, and contractility. 21(14):1790–1802, 2007.

[17] N.J. Bowen et al. Mi-2/nurd: multiple complexes for many purposes. 1677(1-3):52–57, 2004.

[18] B. Manavathi and R. Kumar. Metastasis tumor antigens, an emerging family of multifaceted master coregulators. 282(3):1529–1533, 2007.

[19] A. Simpson et al. Differential expression and subcellular distribution of the mouse metastasis-associated proteins mta1 and mta3. 273(1):29–39, 2001.

[20] Y. Toh, S.D. Pencil, and G.L. Nicolson. A novel candidate metastasis-associated gene, mta1, differentially expressed in highly metastatic mammary adenocarcinoma cell lines. cdna cloning, expression, and protein analyses. 269(37):22958–22963, 1994.

[21] M. Esteller. *DNA methylation, epigenetics and metastasis*, volume 7. Springer Science & Business Media, 2005.

[22] Y. Xue et al. Nurd, a novel complex with both atp-dependent chromatin-remodeling and histone deacetylase activities. 2(6):851–861, 1998.

[23] Y. Zhang et al. Analysis of the nurd subunits reveals a histone deacetylase core complex and a connection with dna methylation. 13(15):1924–1935, 1999.

[24] L. Wang et al. Atrophin recruits hdac1/2 and g9a to modify histone h3k9 and to determine cell fates. 9(6):555–562, 2008.

[25] C.J. Millard et al. Class i hdacs share a common mechanism of regulation by inositol phosphates. 51(1):57–67, 2013.

[26] A.J. Ruijter et al. Histone deacetylases (hdacs): characterization of the classical hdac family. 370(3):737–749, 2003.

[27] J. Taplick et al. Homo-oligomerisation and nuclear localisation of mouse histone deacetylase 1. 308(1):27–38, 2001.

[28] N. Gautam et al. Characterization of molecular interactions between hdac7 and mef2a. *Journal of Biomolecular Structure and Dynamics*, pages 1–10, 2024.

[29] L.S. Dhami et al. Insights from in silico study of receptor energetics of sars-cov-2 variants. 26(11):8794–8806, 2024.

[30] J. Jumper et al. Highly accurate protein structure prediction with alphafold. 596(7873):583–589, 2021.

[31] UniProt Consortium. Uniprot: the universal protein knowledgebase in 2023. *Nucleic Acids Research*, 51(D1):D523–D531, 2022.

[32] J.C. Phillips et al. Scalable molecular dynamics with namd. 26(16):1781–1802, 2005.

[33] J. Huang et al. Charmm36m: an improved force field for folded and intrinsically disordered proteins. 14(1):71–73, 2017.

[34] P.B. Tiwari et al. Covalent complex of dna and bacterial topoisomerase: implications in antibacterial drug development. 15(7):623–631, 2020.

[35] J. Lee et al. Charmm-gui input generator for namd, gromacs, amber, openmm, and charmm/openmm simulations using the charmm36 additive force field. 110(3):641a, 2016.

[36] W. Humphrey, A. Dalke, and K. Schulten. Vmd: visual molecular dynamics. *Journal of Molecular Graphics*, 14(1):33–38, 1996.

[37] E.F. Pettersen et al. Ucsf chimerax: Structure visualization for researchers, educators, and developers. 30(1):70–82, 2021.

[38] X. Zhang, H. Perez-Sanchez, and F.C. Lightstone. A comprehensive docking and mm/gbsa rescoring study of ligand recognition upon binding antithrombin. 17(14):1631–1639, 2017.

[39] X. Zou et al. Recognition of methylated dna through methyl-cpg binding domain proteins. 40(6):2747–2758, 2012.

[40] R. Yin et al. Benchmarking alphafold for protein complex modeling reveals accuracy determinants. 31(8):e4379, 2022.

[41] J. Salamanca Viloria et al. An optimal distance cutoff for contact-based protein structure networks using side-chain centers of mass. 7(1):2838, 2017.